On the Exchange of Momentum over the Open Ocean

James B. Edson,* Venkata Jampana,* Robert A. Weller,[+] Sebastien P. Bigorre,[+]
Albert J. Plueddemann,[+] Christopher W. Fairall,[#] Scott D. Miller,[@] Larry Mahrt,[&]
Dean Vickers,[&] and Hans Hersbach**

*Department of Marine Sciences, University of Connecticut, Groton, Connecticut
[+]Woods Hole Oceanographic Institution, Woods Hole, Massachusetts
[#]NOAA/Environmental System Laboratory, Boulder, Colorado
[@]Atmospheric Sciences Research Center, State University of New York, Albany, New York
[&]College of Earth, Ocean, and Atmospheric Sciences, Oregon State University, Corvallis, Oregon
**European Centre for Medium-Range Weather Forecasts, Reading, United Kingdom

ABSTRACT

This study investigates the exchange of momentum between the atmosphere and ocean using data collected from four oceanic field experiments. Direct covariance estimates of momentum fluxes were collected in all four experiments and wind profiles were collected during three of them. The objective of the investigation is to improve parameterizations of the surface roughness and drag coefficient used to estimate the surface stress from bulk formulas. Specifically, the Coupled Ocean–Atmosphere Response Experiment (COARE) 3.0 bulk flux algorithm is refined to create COARE 3.5. Oversea measurements of dimensionless shear are used to investigate the stability function under stable and convective conditions. The behavior of surface roughness is then investigated over a wider range of wind speeds (up to $25 \, \mathrm{m \, s^{-1}}$) and wave conditions than have been available from previous oversea field studies. The wind speed dependence of the Charnock coefficient α in the COARE algorithm is modified to $\alpha = m U_{10N} + b$, where $m = 0.017 \, \mathrm{m^{-1} \, s}$ and $b = -0.005$. When combined with a parameterization for smooth flow, this formulation gives better agreement with the stress estimates from all of the field programs at all winds speeds with significant improvement for wind speeds over $13 \, \mathrm{m \, s^{-1}}$. Wave age– and wave slope–dependent parameterizations of the surface roughness are also investigated, but the COARE 3.5 wind speed–dependent formulation matches the observations well without any wave information. The available data provide a simple reason for why wind speed–, wave age–, and wave slope–dependent formulations give similar results—the inverse wave age varies nearly linearly with wind speed in long-fetch conditions for wind speeds up to $25 \, \mathrm{m \, s^{-1}}$.

1. Introduction

Investigations of atmospheric turbulence over the world's oceans have shown that the interaction of wind with surface waves results in flow characteristics that differ substantially from a horizontally homogeneous terrestrial surface layer. A simple illustration of this is given by consideration of the surface roughness. Over land, the surface roughness can often be treated as constant or slowly varying as a result of vegetative changes. Over the ocean, the surface roughness or drag is determined by the wave field, which is largely determined by the wind—the stronger the winds, the rougher the seas. Therefore, the exchange of momentum and energy is largely governed by the wave field near the ocean surface.

Above this wave-influenced layer lies a layer where the turbulent flow is governed by the generation of turbulence by wind shear and its generation–suppression by buoyancy–stratification. Many turbulent statistics obey Monin–Obukhov similarity (Obukhov 1971; Monin and Obukhov 1954) in this region, which states that these turbulent statistics are a universal function of z/L after normalization by the appropriate scaling parameters. Here, z is the height above the surface, and L is known as the Monin–Obukhov (MO) length, which represents the height at which the generation of turbulence by shear and buoyancy are equal. A number of studies have shown that MO similarity is valid as long as

Corresponding author address: Dr. James B. Edson, University of Connecticut, Marine Sciences, 1080 Shennecossett Road, Groton, CT 06340.
E-mail: james.edson@uconn.edu

you are in the surface layer above wave influences (e.g., Edson and Fairall 1998; Edson et al. 2004).

As a result, marine meteorologists and physical oceanographers often divide the boundary layer close to the ocean surface into the surface layer where wind shear and buoyancy–stratification govern the turbulent flow (i.e., an MO layer) and a wave boundary layer (WBL) where additional scaling parameters are required for similarity. The search for these scaling parameters, and hypotheses for their use, has been going on for many years (e.g., Charnock 1955; Miles 1957; Hsu 1974; Plant 1982; Geernaert et al. 1986; Donelan 1990; Donelan et al. 1993; Dobson et al. 1994; Hare et al. 1997; Johnson et al. 1998; Bourassa et al. 1999; Drennan et al. 2005), but consensus remains elusive.

This study presents results from several field programs that we specifically designed to investigate the interaction of turbulent flow over surface waves in the marine surface layer. These investigations rely on a set of data collected from the R/P *FLIP* and an offshore tower during the Marine Boundary Layer (MBL; Hristov et al. 2003), Risø Air–Sea Experiment (RASEX; Mahrt et al. 1996), and Coupled Boundary Layers Air–Sea Transfer at Low Winds (CBLAST-LOW; Edson et al. 2007) programs sponsored by the Office of Naval Research. The study also takes advantage of a dataset collected the National Science Foundation (NSF) sponsored Climate Variability and Predictability (CLIVAR) Mode Water Dynamic Experiment (CLIMODE; Marshall et al. 2009) conducted over two winter seasons in the North Atlantic about the northern wall of the Gulf Stream.

The inclusion of the measurements made during CLIMODE allows an investigation of the transfer coefficients at high wind speeds. The CLIMODE momentum fluxes used in this investigation are provided by the direct covariance (DC) technique from two highly instrumented platforms: a moored 2.7-m-diameter foam-hull buoy and a drifting Air–Sea Interaction Spar (ASIS). The ASIS package included a Direct Covariance Flux Systems (DCFS) with a sonic anemometer, infrared hygrometer, and motion correction system that provides estimates of the momentum, sensible heat, and latent heat fluxes using the DC method. The ASIS was deployed during the January 2006 and February 2007 field programs for 10 and 14 days, respectively. A low-power version of the DCFS (without the infrared hygrometer) was deployed for 15 months on the moored buoy, as described by Weller et al. (2012) and Bigorre et al. (2013). The ASIS and buoy used in CLIMODE are shown in Fig. 1.

The combined MBL, RASEX, CBLAST, and CLIMODE dataset covers a wide range of sea states and wage ages. The wave-age parameter c_p/U_{10N}, where U_{10N} is the wind speed at 10 m adjusted to neutral conditions,

and c_p is the phase speed of the waves at the spectral peak, is shown in Fig. 2 for the CLIMODE, CBLAST, and MBL experiments. The value of c_p/U_{10N} for fully developed or mature sea is 1.2 (Donelan 1990), that is, when the phase speed and wind speed are roughly equivalent. This value is shown by the red line in Fig. 2. Wave ages for young (developing) seas are smaller while those for old (decaying) seas associated with swell are larger. The wide range of wave ages associated with the CLIMODE data is consistent with high-latitude wave climatologies for the open ocean. The CBLAST data are representative of an often swell-dominated coastal regime over a three month period, while the MBL data characterize the passage of a single storm over the open ocean. While the fully developed seas occurred most frequently in the composite dataset, there is a significant percentage of data in both young and old seas to investigate the air–sea exchange under a wide range of wind speeds and wave ages.

2. Parameterizations of momentum exchange

The exchange of momentum between the atmosphere and ocean is difficult to measure directly over the ocean. Instead, oceanographers and meteorologists often rely on bulk formulas that relate the fluxes to more easily measured averaged wind speed, temperature, and humidity. These averaged variables are related to the flux through transfer coefficients. For example, based on the dimensional arguments, the exchange of momentum at the ocean surface is expected to scale as the wind speed squared:

$$\tau = -\rho_a \overline{uw} \cong \rho_a C_D U_r^2, \qquad (1)$$

where τ is the momentum flux or surface stress; ρ_a is the density of air; $\rho_a \overline{uw}$ represents the flux computed using the DC method, where u and w are the fluctuating alongwind and vertical velocity components, respectively, and the overbar denotes a time average; U_r is the wind speed relative to water (i.e., the air–water velocity difference); and C_D is the transfer coefficient for momentum known as the drag coefficient. The importance of using relative wind speed is discussed in the appendix. The quadratic relationship between wind speed and surface stress is evident in Fig. 3, which plots DC estimates from the field programs against the relative wind speed adjusted to 10-m.

A widely used parameterization of the drag coefficient is Coupled Ocean–Atmosphere Response Experiment (COARE) algorithm developed during the Tropical Ocean Global Atmosphere (TOGA) COARE (Webster and Lucas 1992) for low to moderate winds

FIG. 1. (left) The 2.7-m foam-hull buoy and (right) ASIS platform used during the CLIMODE program to provide DC estimates of the momentum and heat fluxes. The moored buoy was successfully deployed for 15 months in the Gulf Stream, while the ASIS was deployed for 14 days.

(Fairall et al. 1996). The algorithm was subsequently modified and validated at higher winds in the version known as COARE 3.0 (Fairall et al. 2003). The COARE drag coefficient is parameterized as a function of atmospheric stability, gustiness, and surface roughness as

$$C_D(z/z_0, z/L, G) = \frac{-\overline{uw}}{U_r S_r} = \frac{-\overline{uw}}{U_r^2 G} = \left[\frac{\kappa}{\ln(z/z_0) - \psi_m(z/L)} \right]^2, \tag{2}$$

where z is the height above the surface; κ is the von Kármán constant, z_0 is the aerodynamic roughness length; ψ_m is a dimensionless function that account for the effects of atmospheric stratification; and G is the gustiness parameter given by the ratio of the wind speed S_r to vector-averaged wind U_r (Beljaars and Holtslag, 1991). The gustiness parameter attempts to account for momentum, heat, and mass exchange at very low wind speeds where the vector-averaged wind can vanish, but the average wind speed is nonzero because of gustiness. As a result, shear-driven turbulence produced by these gusts can drive significant exchange in convective conditions (Fairall et al. 1996).

The $\psi_m(z/L)$ function accounts for the departure of the actual wind profile from its semilogarithmic form due to stability. The stability correction that is related to the integral of the dimensionless gradient

$$\phi_m\left(\frac{z}{L}\right) = \frac{\kappa z}{u_*} \frac{\partial U}{\partial z}, \tag{3}$$

where

$$\psi_m\left(\frac{z}{L}\right) = \int_{z_0}^{z} \left[1 - \phi_m\left(\frac{z}{L}\right) \right] \frac{d(z/L)}{z/L}, \tag{4}$$

and $u_* \equiv (-\overline{uw})^{1/2}$ is the velocity scaling parameter known as the friction velocity. Determination of the dimensionless shear, and flux–profile relationships in general (e.g., Edson et al. 2004), requires fluxes and their associated gradients.

a. Dimensionless shear

Flux–profile measurements were made during the RASEX, MBL and CBLAST programs that utilized two oversea towers and the R/P *FLIP* as shown in Fig. 4. The setups used on the RASEX and CBLAST towers are
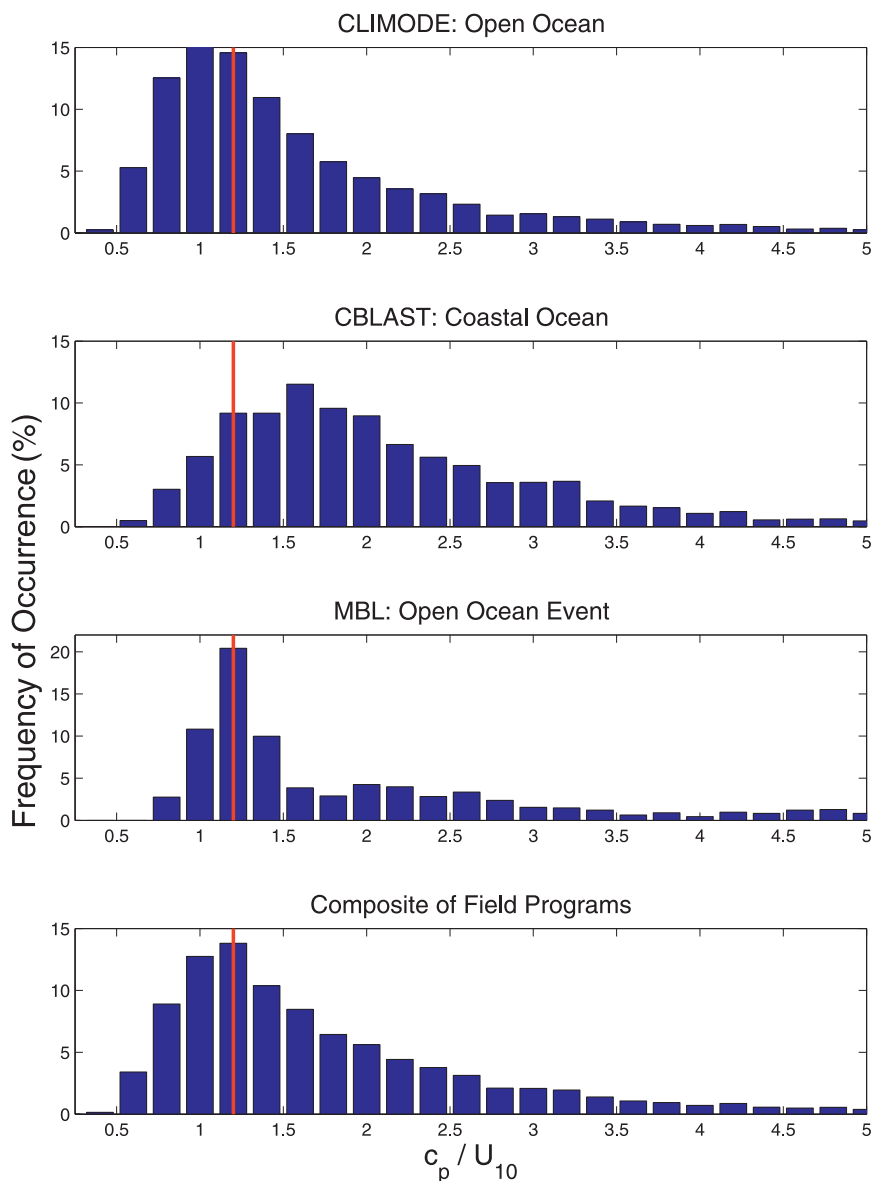
FIG. 2. The frequency of occurrence of wave ages from (top three rows) different field programs: CLIMODE, CBLAST, and MBL. The solid red line is for a wave age of 1.2 that is commonly associated with fully developed seas. Values <1.2 indicate developing (young) seas, while values >1 indicate decaying (old) seas. (bottom) Composite of all the data.

described by Vickers and Mahrt (1999) and Edson et al. (2007), respectively. Briefly, the RASEX results are limited to the "long"-fetch (i.e., fetches >15 km) conditions discussed in Mahrt et al. (1996) where the water depth is approximately 3 m at the tower. The cup anemometers used in this study were positioned at 7, 15, 20, 29, and 38 m above mean sea level. A 10-min averaging time was used to compute the fluxes from 3-axis sonic anemometers located at 6, 10, 18, and 32 m.

The CBLAST results are restricted to wind directions between 190° and 245° to provide "infinite" fetch and minimize the flow distortion by the tower, which faces the open ocean to its south. The water depth is approximately 15 m at the tower. A profiling mast (Fig. 1) supporting a moving sensor package holding a 2-axis sonic anemometer was used to measure the wind speed at approximately 3, 5, 7, 10, 13.5, and 15.5 m after adjustment for tides. The array was used to calibrate 3-axis sonic anemometers deployed at fixed locations of approximately 4, 6.5, 10, 15, 18, and 20 m. A 20-min average was used to compute the fluxes in unstable conditions, while the average of two 10-min-averaged fluxes was used in stable conditions.
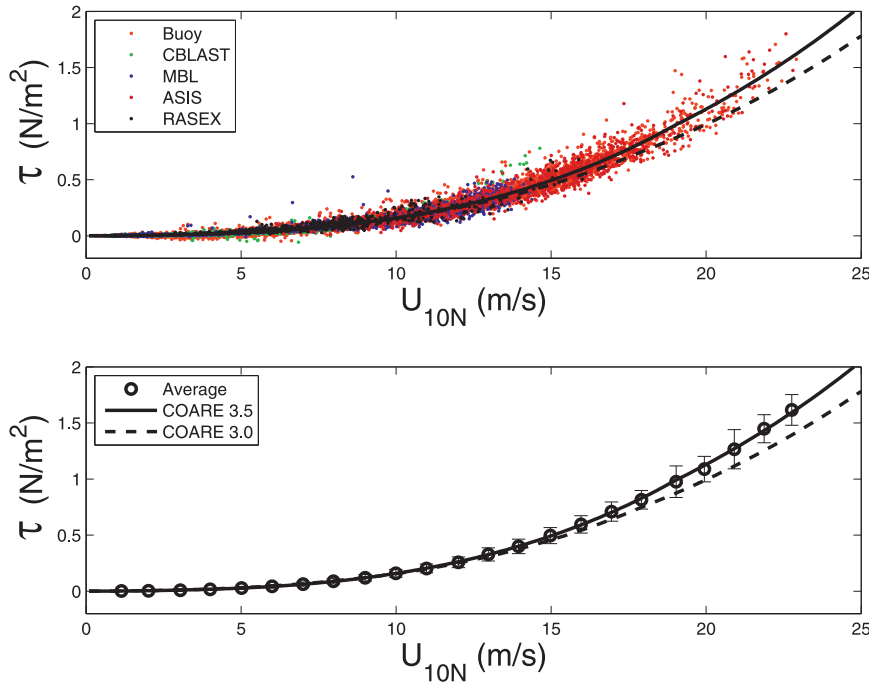
FIG. 3. Direct estimates of the momentum flux (surface stress) vs relative wind speed adjusted to 10 m and neutral stability from four field programs and five platforms. No ship data are included in the analysis to reduce the effect of flow distortion. (top) The individual flux estimates from each experiment and (bottom) the data averaged over wind speed bins. The dashed line represents the original COARE 3.0 bulk algorithm and the solid black line is the modified COARE 3.5 algorithm, as described in the text.

The MBL results are limited to a 7-day period with optimal winds from the northwest as described by Friehe et al. (2001). The setup shown in Fig. 4 for the R/P *FLIP* consisted of a vertical array of five 3-axis sonic anemometers to measure momentum and buoyancy fluxes

at approximately 4, 5, 9, 14, and 18 m above mean sea level. Eleven cup/vane anemometers were used to measure the mean wind speed between 3 and 17 m above the ocean surface. The cup–vane pairs located on either side of the R/P *FLIP*'s port boom were excluded from

FIG. 4. The three platforms used to directly measure flux–profile relationships during the CBLAST, MBL, and RASEX programs. (left) The ASIT tower used in CBLAST where the profiling mast is at far left and the mast holding the fixed sensors is nearer the platform. (middle) The R/P *FLIP* used in MBL and (right) the tower used in the RASEX program.
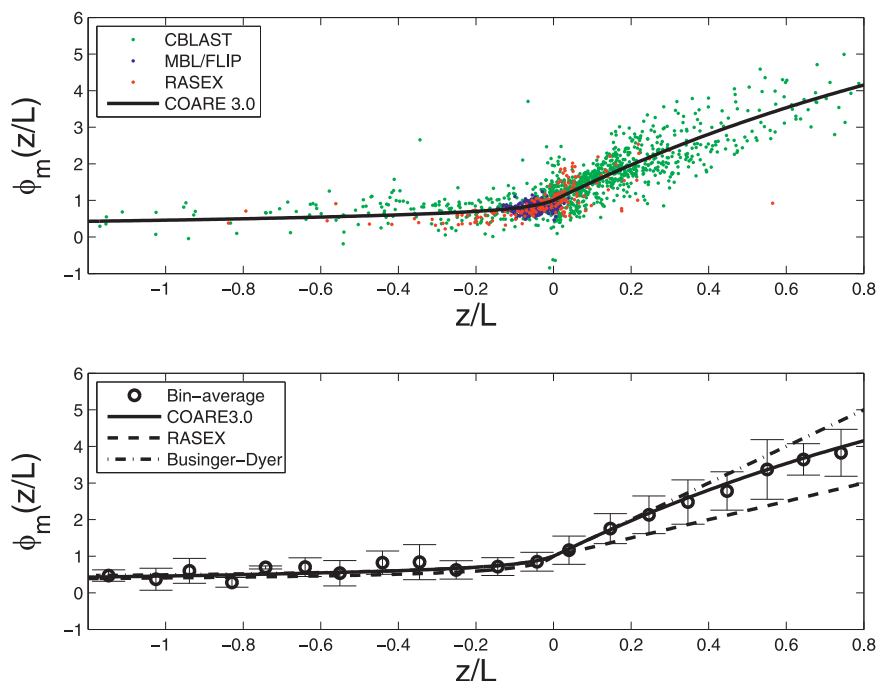
FIG. 5. (top) Individual estimates of the dimensionless shear vs the stability parameter z/L from the RASEX, MBL, and CBLAST programs for $c_p/U_{10N} < 2.5$. (bottom) Bin-averaged estimates of the combined data plotted against several parameterizations presented in the literature. The solid black line represents the COARE 3.0 parameterization used to correct for stability effects in this investigation.

the analysis because of flow distortion. The remaining nine cup anemometers were locate at approximately 2.9, 3.8, 4.7, 5.6, 6.8, 7.8, 12.7, 14.7, 15.7, and 16.2 m above mean sea level. These remaining cups were corrected for over speeding and the sonics were motion corrected as described by Edson et al. (1998) and Miller et al. (2008). A 15-min average is used to compute the fluxes. The 10–20-min averaging times in these experiments are chosen to maximize the correlation between mean wind speed and wind stress (Mahrt et al. 1996), but are short enough to limit the impact of nonstationarity on the fluxes.

As shown in Fig. 2, the CBLAST data are often characterized by old seas with low wind conditions over swell. A number of studies (e.g., Smedman et al. 1994, 1999) have shown that swell can have a significant impact on wind profiles under these conditions. For example, the large-eddy simulations (LES) conducted by Sullivan et al. (2008) show that fast moving swell can impact the wind profiles throughout the surface layer under light wind conditions. Therefore, the data used in the following investigation of the dimensionless shear is limited to wave ages c_p/U_{10N} less than 2.5. This both limits the impact of swell and removes much of the uncertainty associated with flux and profile measurements under very light wind conditions.

In all experiments, the wind shear was calculated from a least squares fit to U versus $\ln(z)$ using a second-order polynomial. The dimensionless shear was computed using the local values of the momentum flux and MO length as described by Vickers and Mahrt (1999). The dimension shear was computed at the sonic anemometer heights of 6 and 10 m for RASEX; 4, 6.5, and 10 m for CBLAST; and 5 m for FLIP. Although the depth of the WBL for momentum exchange is not universally defined—for example, see the discussions in Chalikov (1986, 1995), Belcher and Hunt (1993), Mastenbroek et al. (1996), Kudryavtsev et al. (2001), Moon et al. (2004), and Chalikov and Rainchik (2011)—these heights are expected to be within the surface layer and generally above the WBL for $c_p/U_{10N} < 2.5$.

Measurements of the dimensionless shear from the RASEX, MBL, and CBLAST experiments are shown in Fig. 5. The bin-averaged data agree very well with the current formulations used in the COARE 3.0 algorithm (Fairall et al. 2003), which is based on the Kansas (Businger et al. 1971) and over ice Surface Heat Budget of the Arctic Ocean (SHEBA) (Persson et al. 2002) experiments. The agreement with the commonly used Businger–Dyer formulations (Businger 1988) in unstable conditions is not surprising since this form of the dimensionless shear

has been successfully used to compute bulk fluxes over the oceans for decades. A fit to the data between $|z/L| < 0.04$ and the mean of the data between $|z/L| < 0.01$ both provide a von Kármán constant of 0.40, which is the most commonly assigned value in the literature.

There is more uncertainty in the dimensionless shear under stable conditions, but the same can be said for surface layers over land. The average data follow the Businger–Dyer function out to $z/L \sim 0.5$ but then increase less rapidly. The COARE 3.0 algorithm relies on the formulation presented by Beljaars and Holtslag (1991) for stable conditions, which models the roll off under highly stable conditions using several tunable parameters. The values used in the COARE 3.0 function agree well with the bin-averaged data as shown in Fig. 5. It should be noted that the data do not compare well with the RASEX parameterization under stable conditions reported by Vickers and Mahrt (1999). However, this discrepancy is effectively removed by limiting the data to wind directions that provide long fetch. This restriction is believed to remove many of the complications that arise because of surface-layer adjustment from land to sea over short fetch as described in Mahrt et al. (1998, 2001).

The agreement between the individual datasets and previously used parameterizations strongly suggests that the use of flux–profile relationships based on MO similarity is valid in the marine surface layer for c_p/U_{10N} less than 2.5. However, there are small differences between the COARE 3.0 algorithm and the data over all stability conditions. For example, the bin-averaged values of the dimensionless shear under unstable conditions are slightly lower than COARE 3.0 in near-neutral conditions and fall above and below the line for more convective conditions. In fact, the average data fall between the COARE 3.0 algorithm and the parameterizations reported by Vickers and Mahrt (1999) in near-neutral conditions.

This suggests that the data may still be influenced by waves, which violates the assumptions made for MO similarity. For example, upon close examination of the individual datasets, the RASEX data taken over shallow water with generally younger sea conditions fall slightly below the CBLAST and FLIP taken under more mature sea conditions. However, these differences are subtle, and an investigation on the impact of surface waves on shear production is ongoing. Therefore, for the remainder of this investigation, it is assumed that the measurements are generally made above the WBL (i.e., for $z \geq 4\,\mathrm{m}$) and that MO similarity is valid. Stability corrections are made using the COARE 3.0 algorithm.

b. Neutral drag coefficient

The results from section 2a suggest that our measurements are above the WBL. However, this does not

mean that surface waves do not strongly impact momentum exchange over the ocean. In fact, once the sea becomes fully rough, the waves are expected to have a first-order impact on momentum exchange as roughness elements. As such, waves strongly impact the lower boundary condition of the wind profile (i.e., the roughness length) even if they do not strongly impact the shape of the wind profile. In this study, the role of surface waves in momentum exchange through surface roughness is investigated using the neutral drag coefficient defined as

$$C_{DN}(z/z_0) = \frac{-\overline{uw}}{U_N^2 G} = \left[\frac{\kappa}{\ln(z/z_0)} \right]^2, \quad (5)$$

where the subscript N denotes neutral atmospheric stratification. The DC measurements of the momentum flux are combined with stability-corrected wind speeds to directly compute the neutral drag coefficient. These measurements can then be used to develop parameterization of the flux in terms of the surface roughness as done in this investigation.

The COARE algorithm parameterizes the surface roughness by separating it into two terms

$$z_0 = z_0^{\mathrm{smooth}} + z_0^{\mathrm{rough}}, \quad (6)$$

where z_0^{smooth} accounts for "roughness" of the ocean when it is aerodynamically smooth and the surface stress is supported by viscous shear. The second term z_0^{rough} accounts for the actual roughness elements driven by the wind stress in the form of surface gravity waves (e.g., Liu et al. 1979; Smith 1988; Fairall et al. 1996). The smooth-flow component of the total roughness is often parameterized in terms of the roughness Reynolds number (i.e., the ratio of the inertial to viscous forces), which results in

$$z_0^{\mathrm{smooth}} = \gamma \frac{\nu}{u_*}, \quad (7)$$

where ν is the kinematic viscosity, and γ is the roughness Reynolds number for smooth flow, which has been determined to be 0.11 from laboratory experiments. The rough-flow component is often parameterized using the scaling proposed by Charnock (1955):

$$z_0^{\mathrm{rough}} = \alpha \frac{u_*^2}{g}, \quad (8)$$

where α is Charnock coefficient, and g is the gravitational acceleration. The Charnock coefficient is the normalized roughness and takes the dimensionless form of an inverse Froude number as it represents the ratio of

the gravitational restoring force to the inertial forces (i.e., the wind stress) generating the roughness elements. As such, this parameterization represents the roughness of the wind waves, which support a significant fraction of the surface stress as the surface transitions to fully rough.

The combination of the viscous and wave-induced stresses is often used to define the total surface stress:

$$\tau = \tau_\nu + \tau_w, \tag{9}$$

where τ_ν and τ_w are the viscous and wave-induced components, respectively. The viscous stress supports most of the momentum exchange at wind speeds below $3\,\mathrm{m\,s^{-1}}$. The surface waves support most of the surface stress via form drag (normal stress) once the sea becomes fully rough, which occurs for wind speeds above approximately $7.5\,\mathrm{m\,s^{-1}}$ (Donelan 1990). Between these two extremes lies a transitional regime (Kraus and Businger 1994) where the surface waves support a substantial fraction of the stress (Banner and Peirson 1998). It should be noted, however, that while these stress components are additive, the drag coefficients defined by the individual roughness components are not, that is,

$$
\begin{aligned}
C_{DN}(z/z_0) &= \left[\frac{\kappa}{\ln(z/z_0)}\right]^2 \\
&\neq \left[\frac{\kappa}{\ln(z/z_0^{\mathrm{smooth}})}\right]^2 + \left[\frac{\kappa}{\ln(z/z_0^{\mathrm{rough}})}\right]^2. \tag{10}
\end{aligned}
$$

Therefore, the individual roughness lengths cannot be used to directly estimate the stress components. Instead, the COARE algorithm uses these parameterizations to estimate the total roughness

$$z_0 = \gamma \frac{\nu}{u_*} + \alpha \frac{u_*^2}{g}, \tag{11}$$

which is then used to compute the drag coefficient and the total stress using (1) and (2) as described by Fairall et al. (2003).

The investigation will focus on the parameterization of the rough-flow component through the Charnock coefficient. This coefficient was originally referred to as the Charnock constant but is now known to vary as a function of, for example, wind speed, wave age, and sea state. The behavior of the Charnock coefficient as a function of wind speed is investigated in section 2c. This is followed by investigations of the wage-age and sea-state dependence of the Charnock coefficient in sections

2d and 2e; where wave age quantifies the stage of wave development, while sea state characterizes the current conditions in term of, for example, wave height, wave period, and wave steepness. The investigation then provides a means to reconcile the wind speed– and wave age–dependent formulation over the open ocean in section 3, and discusses their behavior at high and low winds in sections 3a and 3b. The investigation concludes with a summary that includes a comparison of the DC momentum fluxes versus the parameterizations developed in this study in section 3c.

c. Wind speed–dependent formulation

In the COARE 3.0 algorithm (Fairall et al. 2003), the roughness length due to z_0^{rough} is parameterized using a wind speed–dependent formulation:

$$\alpha = \frac{g z_0^{\mathrm{rough}}}{u_*^2} = f_1(U_{10N}), \tag{12}$$

where α is a function of wind speed, and U_{10N} is the wind speed at 10 m under neutral conditions. Direct estimates of the stability-corrected (neutral) drag coefficient are shown in Fig. 6 along with the COARE 3.0 parameterization, which blends the smooth- and rough-flow parameterization given by (11). The combination of the smooth-flow parameterization that increases with decreasing wind and a rough-flow parameterization that increases with increasing wind results in a minimum in the total roughness. Kraus and Businger (1994) predict that the roughness length and thereby the drag coefficient are expected to have a minimum for u_* between 0.07 and $0.11\,\mathrm{m\,s^{-1}}$, which corresponds to a wind speed between 2 and $3\,\mathrm{m\,s^{-1}}$. There is clear evidence for this minimum in Fig. 6.

The neutral drag coefficients are in good agreement with COARE 3.0 over moderate wind conditions. However, there are differences at the lowest and highest wind speeds where COARE 3.0 over- and underestimates the drag, respectively. Therefore, the combined dataset is used to refine the dependence of the Charnock coefficient as a function of wind speed. This is accomplished through the following steps.

1) Individual estimates of the neutral drag coefficients at 10 m are computed from measurements following (5) as shown by the upper panel of Fig. 6.
2) The measured C_{D10N} are then averaged into $1\,\mathrm{m\,s^{-1}}$ bins of U_{10N} as shown by the middle panel of Fig. 6.
3) Likewise, the measurements of $\overline{uw}$ are separately bin averaged according to U_{10N} to reduce some of the self correlation between these variables.
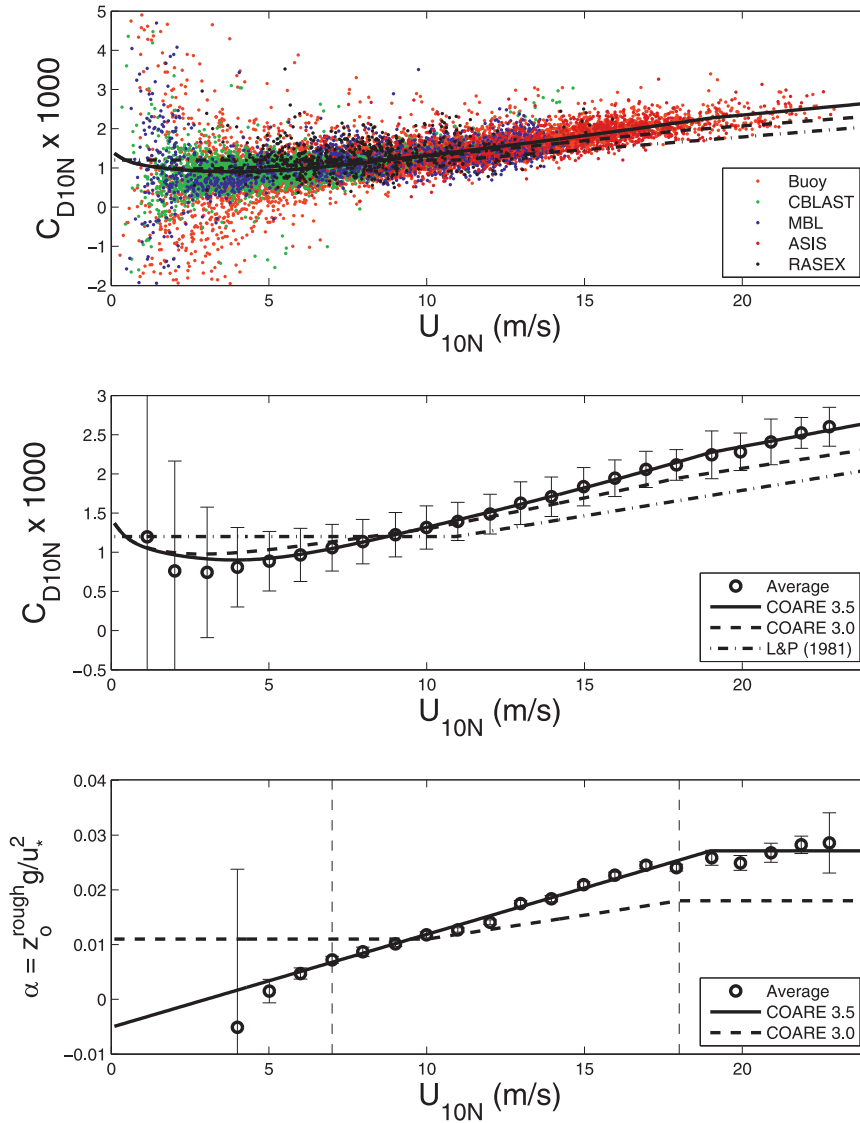
FIG. 6. (top),(middle) Direct estimates of the drag coefficient plotted vs relative wind speed. The values have been adjusted to 10 m and corrected for atmospheric stability using MO similarity theory (Fairall et al. 2003). (top) The individual data from each platform. (middle) The bin-averaged drag coefficients vs wind speed where the error bars represent the standard deviation about the mean. The dashed line represents the COARE 3.0 algorithm, while the solid line is a modification to this algorithm designated as COARE 3.5. The dashed–dotted line is the function provided by Large and Pond (1981). (bottom) Estimates of the Charnock coefficient averaged over wind speed bins. The error bars represent the standard error about the mean.

4) The bin-averaged values of $\overline{uw}$ are used to compute the friction velocity.
5) The bin-averaged drag coefficients and friction velocities are used to compute the roughness length for rough flow from $z_0^{\text{rough}} = z_0 - z_0^{\text{smooth}} = 10e^{-\kappa/\langle C_{D10N}^{1/2} \rangle} - \gamma\nu/u_*$.
6) The roughness length and friction velocities are used to compute the Charnock coefficient from $\alpha = gz_0^{\text{rough}}/u_*^2$ as shown in the lower panel of Fig. 6.

The COARE 3.0 algorithm is found to underestimate the observed surface stresses and Charnock coefficients at high winds and overestimate these values at low winds. Therefore, the bin-averaged estimates of the Charnock coefficients are used to improve the performance of the wind speed–dependent parameterization. This is accomplished by fit to the average data between 7 and 18 m s^{-1} given by

$$\alpha = mU_{10N} + b, \tag{13}$$

where $m = 0.017 \, \text{m}^{-1} \, \text{s}$, and $b = -0.005$. The lower limit is selected based on the assumption that the sea becomes fully rough above this value. Note that the values of the roughness length fall off rapidly at wind speeds below $5 \, \text{m} \, \text{s}^{-1}$ because of the removal of z_0^{smooth}. The upper limit is selected based on the observation that the Charnock coefficient appears to level off above this value and can be modeled by a constant value given by $\alpha_{\text{max}} \approx 0.028$. Additionally, the combination of the modified rough-flow parameterization with the smooth-flow parameterization given by (7) gives better agreement with the roughness at low wind speeds than currently parameterized in COARE 3.0. As a result, the new parameterization designated as COARE 3.5 provides good agreement with the merged dataset over the wide range of wind speeds.

d. Wave age–dependent formulation

Another common approach to modeling the drag coefficient is to parameterize the surface roughness as a function of wave age using either c_p/u_* or c_p/U_{10N}. For example, a number of investigators (e.g., Kitaigorodskii, 1973; Geernaert et al. 1986; Nordeng 1991; Oost et al. 2002) have proposed a wave age–dependent Charnock coefficient

$$\alpha = \frac{u_*^2 z_0^{\text{rough}}}{g} = f_2\left(\frac{u_*}{c_p}\right), \tag{14}$$

where α is now a function of inverse wave age. Measurements show that the ocean is typically rougher for younger waves at any given wind speed. Therefore, one might expect a wave age–dependent drag coefficient to provide a better estimate of the surface drag than a wind speed–dependent formulation. In fact, researchers commonly attribute some of the scatter in drag coefficient versus wind speed (e.g., Fig. 6) to processes that cannot be represented by the wind speed alone such as the duration of a wind event, the fetch over which the wind is blowing, the depth of the water, etc.—all of which affect the wave age.

Smith et al. (1992), Johnson and Vested (1992), Johnson et al. (1998), and Oost et al. (2002) have all attempted to account for the wave age dependence by an empirically derived Charnock coefficient in the general form

$$\alpha = f_2\left(\frac{u_*}{c_p}\right) = A\left(\frac{u_*}{c_p}\right)^B, \tag{15}$$

where A and B are coefficients determined by fits to the data. Since u_* appears in the definition of α and the wave age, these investigations acknowledged the possibility that self-correlation could give rise to spurious results (e.g., Hicks 1978; Dobson et al. 1994). Johnson et al. (1998) argued that this effect could be reduced by comparing the mean results from several sites with different fetches, such that their coefficients are derived from a fit to the mean phase speed and Charnock coefficients from a number of different field experiments.

This analysis relies on the wide range of wage ages captured during CBLAST and CLIMODE deployments and, to a lesser extent, the wind event captured during the MBL experiment to reduce the problem of self-correlation (Donelan et al. 1992; Lange et al. 2004; Drennan et al. 2005). The Charnock coefficient is computed using individual estimates of the drag coefficient and friction velocity using steps 5) and 6) as in section 2c. The natural log of the Charnock coefficient $\ln(\alpha)$ is then averaged in 0.025 wide bins of $\ln(u_*/c_p)$ using only data where $U_{10N} > 6 \, \text{m} \, \text{s}^{-1}$. The individual and bin-averaged values of the Charnock coefficient produced this way are shown in the upper panel of Fig. 7.

As in previous studies, the Charnock coefficient is seen to increase with inverse wave age reflecting the commonly held view that the younger the waves, the rougher the surface. Research has shown that a fully developed sea occurs at $u_*/c_p \approx 0.03$, that is, where $c_p/u_* \approx 32$, and $c_p/U_{10N} \approx 1.2$ (Donelan 1990). A linear fit to bin-averaged values of $\ln(\alpha)$ to $\ln(u_*/c_p)$ for $u_*/c_p > 0.03$ using the DC estimates gives $A = 0.114$ and $B = 0.622$. The use of these coefficients with (15) results in the solid line labeled COARE 3.5 drawn in Fig. 7.

These open-ocean values provide significantly less variability in the Charnock coefficient than the coefficients reported in shallow water and fetch-limited environments by Smith et al. (1992), Johnson et al. (1998), and Oost et al. (2002) as shown by the middle panel in Fig. 7. These coefficients have generally been tuned to data over a narrow range of wave ages. However, Charnock coefficients determined experimentally over the ocean generally range from 0.011 to 0.018 from fully developed seas (Kraus and Businger 1994). As shown in Fig. 7, the COARE 3.5 parameterization spans that same range for $43 > c_p/u_* > 20$ (i.e., $0.02 < u_*/c_p < 0.05$), which are values commonly found over the open ocean. The parameterization gives a value of $\alpha = 0.013$ at the fully developed value of $c_p/u_* = 32$. The same cannot be said of the other functions, which tend to be unrealistically low for mature seas and unrealistically high for young seas. The one exception is the formulation given by Smith et al. (1992) that agrees reasonably well with COARE 3.5 over the range $0.02 < u_*/c_p < 0.05$.
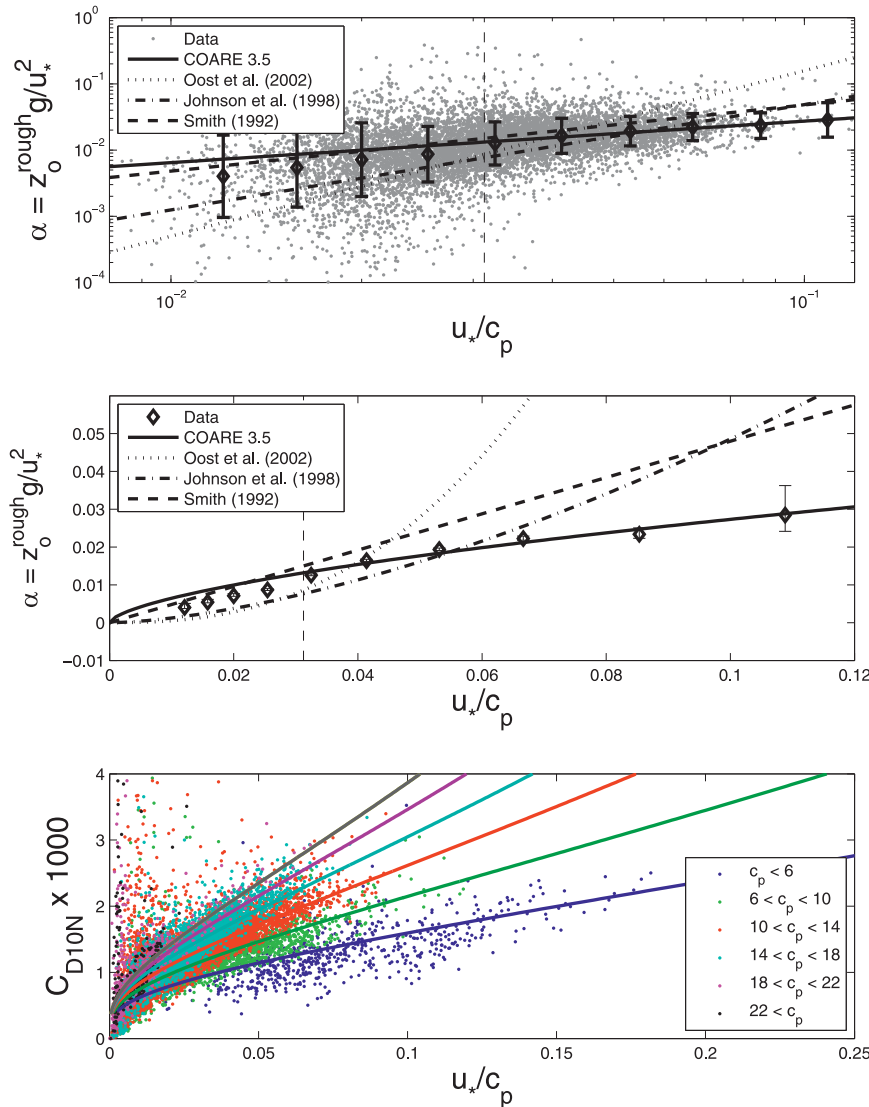
FIG. 7. (top) Individual and bin-averaged estimates of the Charnock coefficient vs inverse wave age where the error bars represent the standard deviation about the mean. (middle) The bin-averaged data on a linear scale. The error bars represent the standard error about the mean. The solid line is a fit to the data using (15), while the other lines present previously reported relationships as labeled. The dashed vertical line represents the fully developed value of inverse wave age. (bottom) All of the observations found over the narrow range of phase speeds (m s^{-1}) vs inverse wave age. The lines representing the COARE 3.5 function are then generated by fixing the phase speed in the middle of each range and allowing the friction velocity to vary.

Obviously, the value of the wave age and therefore the value of the Charnock coefficient can be driven by variability in u_*, which is largely a function of wind speed, and/or c_p, which is largely a function of wind duration, fetch, and water depth. By limiting the CBLAST data to open-ocean wind directions, nearly all of these data can be characterized by deep water and infinite fetch. Therefore, wave age is primarily driven by the duration of wind events; while bottom friction and fetch

have little or no impact. The single mechanism driving wave age in the open-ocean dataset results in similar drag coefficients for similar wave ages in each field experiment. As a result, the function does a good job of explaining the spread of data when c_p is held constant over a wide range of u_* as shown by the solid lines in the bottom panel of Fig. 7. Similar agreement is found when u_* is held constant and c_p is allowed to vary over the range shown in the legend.

The RASEX data were not included in the bin-averaged results because they did not exhibit similar drag coefficients at the same inverse wave ages of the other datasets. The RASEX experiments were conducted in shallow water where bottom friction drives much of the variability in u_*/c_p (Johnson and Kofoed-Hansen 2000). Specifically, the RASEX stress estimates are similar to those in the other experiments, but bottom friction and fetch limitations result in smaller phase speeds, which corresponds to younger seas. However, the COARE 3.5 function does a good job of modeling the drag coefficients for the RASEX experiment. For example, the RASEX data are included in the bottom panel of Fig. 7, and are responsible for most of the youngest waves data (i.e., the blue dots where $c_p < 6 \, \text{m s}^{-1}$). This suggests that (15) may also be applicable to shallow water and fetch-limited environments. This is explored further in section 3c.

e. Sea state– and wave age–dependent formulation

The Charnock coefficient represents the ratio of gravitational accelerations to inertial accelerations, which is analogous to an inverse Froude number as discussed in section 2b. The wave Froude number can be expressed in terms of the wave slope (Kraus and Businger 1994)

$$\text{Fr}_w = (Hk)^2, \tag{16}$$

where H is the wave amplitude. Therefore, it may be more appropriate to parameterize the Charnock coefficient as a function of wave slope, for example,

$$\alpha = f_3(\sigma_H k_p), \tag{17}$$

where σ_H is the significant wave height, and k_p is the wavenumber of the dominant waves. For example, Donelan et al. (1993) present an alternative approach that scales the roughness length by the significant wave height. The scaled roughness length z_0/σ_H expresses the ability of the waves to serve as roughness elements (Donelan 1990). Donelan (1990), Smith et al. (1992), Dobson et al. (1994), and Martin (1998) have conducted investigations by deriving relationships between the scaled roughness and wave age c_p/U_N. These investigations gave reasonable agreement among four independent experiments, which ranged in environmental conditions from a lake to the open ocean. This suggests that this scaling approach may be a good candidate for the development of a universal relationship between sea state, wave age, and aerodynamic roughness.

The link between this approach and the wave slope–dependent Charnock coefficient is easily demonstrated by assuming a linear relationship in (17)

$$\frac{g z_0^{\text{rough}}}{u_*^2} = D \sigma_H k_p, \tag{18}$$

where D is a numerical constant. The deep-water dispersion relationship can then be used to rewrite (18) as

$$\frac{z_0^{\text{rough}}}{\sigma_H} = D \left(\frac{u_*}{c_p}\right)^2 \tag{19}$$

a form of which was originally derived by Hsu (1974) using similar arguments. The combined data from CBLAST, CLIMODE, and the MBL are used to plot the scaled roughness versus wave age in Fig. 8. Individual estimates of the roughness lengths are computed and bin averaged as in section 2c. The fit to the bin-averaged data for $u_*/c_p > 0.03$ give an exponent of 2.02 and a numerical constant of 0.091. The exponent is remarkable close to the value of 2 found in (19) for the linear relationship given by (18) and by Hsu (1974). In fact, a value of $D = 0.09$ in (19) gives good agreement with the data over all sea states. This value is smaller than the constant reported by Hsu (1974), which may be due to the preponderance of laboratory data used in his study. However, this value gives good agreement with the formulation given by Donelan (1990), which was based on a number of field experiments, except over the youngest seas. It is shown in section 3c that the Donelan (1990) formulation gives slightly more uncertainty than (19) with $D = 0.09$ when compared to DC estimates of the flux. Therefore, the value of $D = 0.09$ is used in (18) to model the effect of both wage age and sea state in COARE 3.5.

3. Reconciling wind speed– and wave age–dependent formulations

It is not always easy to compare drag coefficients based on wind speed with those based on wave age and/or wave slope because of the potential mismatch between atmospheric forcing and the state of the underlying sea. As such, comparisons of wave age–dependent drag coefficients are commonly plotted as a family of curves versus a single wind speed–dependent formulation. However, the European Centre for Medium-Range Weather Forecasts (ECMWF) has determined a wind speed–dependent drag coefficient based on the wave age–dependent surface roughness computed with their coupled atmospheric–wave model (Hersbach 2011). The wind speed–dependent formulation is given by

$$C_{DN} = [c_1 + c_2(U_{10N})^{p_1}]/(U_{10N})^{p_2}, \tag{20}$$

where $c_1 = 1.03 \times 10^{-3}$, $c_2 = 0.04 \times 10^{-3}$, $p_1 = 1.48$, and $p_2 = 0.21$. The drag coefficient therefore represents
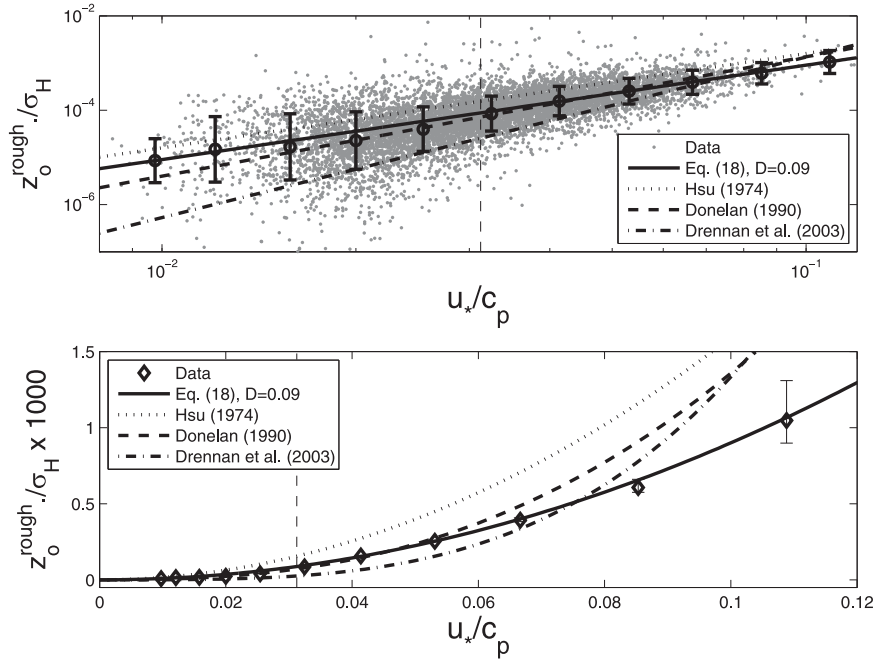
FIG. 8. The surface roughness scaled by significant wave height averaged over inverse wave age bins. The error bars represent (top) the standard deviation and (bottom) the standard error about the mean. The solid line is from (19) with $D = 0.09$, while the other lines present previously reported relationships as labeled. These parameterizations are normalized by the significant wave height using $\sigma_H = 4\sigma$ as appropriate where σ is the RMS value used in some of the previous studies. The dashed vertical line represents the fully developed value of inverse wave age.

globally averaged wave age–dependent roughness at a given wind speed. This function is plotted versus wind speed in Fig. 9. The agreement between the measurements and the ECMWF parameterization is remarkable given the range of wave age conditions encountered in our datasets as shown in Fig. 2.

Perhaps more surprising is the agreement between ECMWF and the COARE 3.5 algorithm given the nature of the two parameterizations. Specifically, it has been argued that some of the discrepancy between bulk estimates and direct measurements of the fluxes reflect the variability in wave properties at any given wind speed. However, the COARE algorithm matches the observations well without any wave information. Furthermore it is nearly identical to the function representing the globally averaged drag coefficient from the wave age–based model. This begs the following question: why do wave age– and wind speed–dependent formulation give such similar results?

The answer is found by looking at the relationship between inverse wave age and wind speed shown in Fig. 9. The measurements indicate that fully developed seas ($u_*/c_p \approx 0.03$, shown by the broken line in Fig. 9) are not commonly observed over the open ocean. This is consistent with the histograms shown in Fig. 2, where the composite indicates that fully developed seas occur about 12% of the time. The relationship between wind speed and inverse wave age is quite linear over a wide range of wind speeds, as seen clearly in the bin-averaged data (middle panel of Fig. 9). Presumably, the strong winds found under midlatitudes storms simply do not remain over the same group of waves long enough to become fully developed as a result of the different propagation speeds of the storm and wave field. It can also be argued that the stronger the forcing, the longer it takes to reach full development. For example, the observations shown in Fig. 9 suggest that storms with winds between 8 and 12 m s^{-1} are strong enough to overcome the background swell and persist long enough over a region of the ocean for the waves to reach full development. Similar behavior was reported in Taylor and Yelland (2001) for data collected during the Humidity Exchange Over the Sea (HEXOS; Smith et al. 1992) and Storm Wave Study experiments (SWS-2; Dobson et al. 1994, 1999).

Despite approximate linearity for wind speeds of 5–18 m s^{-1} the third-order fit provides a better fit to the averaged data. Therefore, the third-order relationship
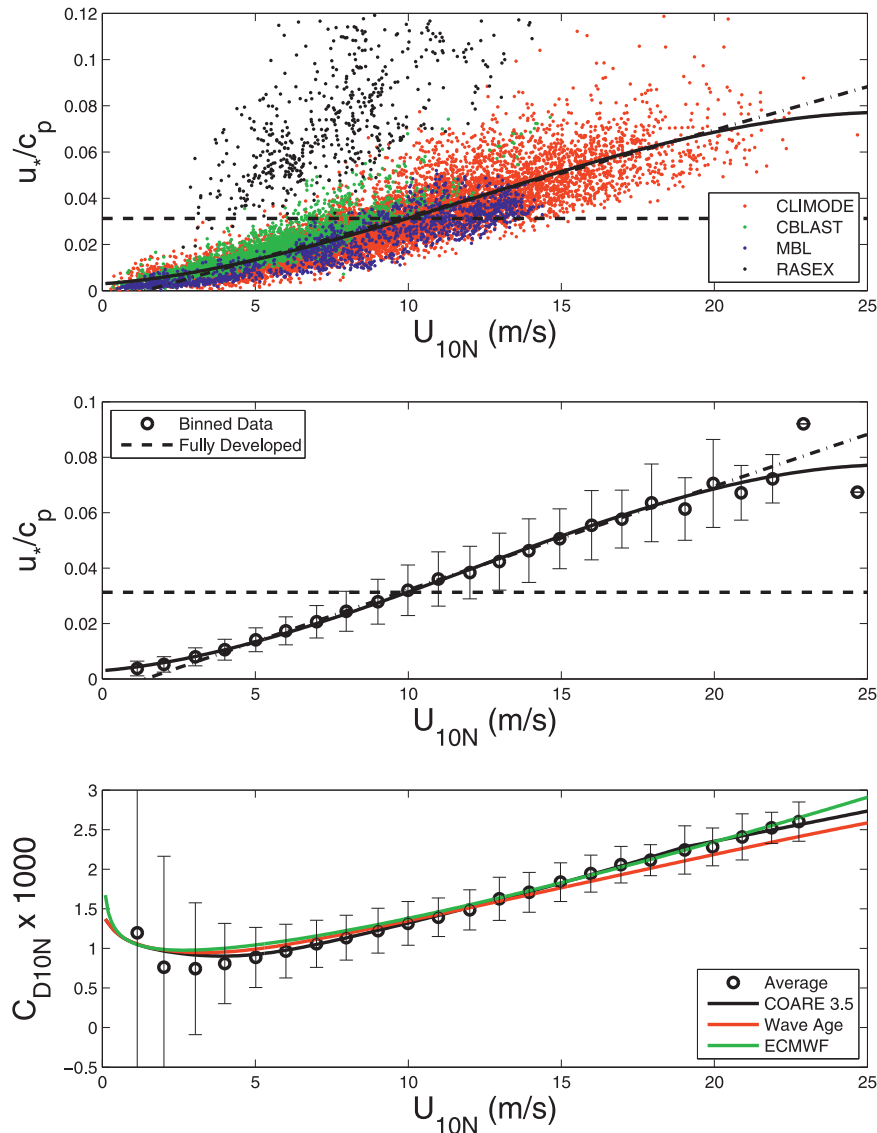
FIG. 9. Inverse wave age plotted vs relative wind speed. (top) The individual data from each experiment, and (middle) the data averaged over wind speed bins. The RASEX data are not included in this average. The dashed black line represents the inverse wave age commonly associated with fully developed seas. The dashed–dotted line is a linear fit to the averaged data, while the solid line is a third-order fit. (bottom) As in Fig. 6, but with the addition of the green line representing the function derived by ECMWF as given by (20), and the red line that combines the third-order fit with (15).

between inverse wave age and wind speed can be used to convert the wave age–dependent roughness length given by (15) to a wind speed–dependent roughness length:

$$\alpha = f_2(u_*/c_p) \Rightarrow u_*/c_p = g(U_{10N}) \Rightarrow$$

$$\alpha = f_2[g(U_{10N})] \approx \alpha = f_1(U_{10N}). \qquad (21)$$

The resulting wind speed–dependent roughness length closely matches the COARE 3.5 parameterization.

However, the shallow-water RASEX data clearly do not obey the ocean-ocean relationship between U_{10N} and u_*/c_p. There also appears to be a growing discrepancy between this relationship and the CBLAST data with increasing wind speed, which is likely due to the impact of bottom friction as the waves grow in size. Therefore, the inverse wave age versus wind speed relationship is only expected to hold under open-ocean conditions.

The third-order fit also highlights the observation that the wage age goes to a finite positive value under very low wind conditions because of the ubiquitous nature of swell (Hanley et al. 2010) and the role of gustiness in maintaining momentum exchange under these conditions (Fairall et al. 1996). Perhaps more importantly, the fit also supports the idea (e.g., Hsu 1974) that the wave field saturates at high wind conditions. The behavior of momentum exchange at extremely high and very low winds is explored further in the following sections.

a. High wind speeds

The measured drag coefficients are larger than a number of previous open-ocean formulas such as Liu et al. (1979), Large and Pond (1981), and Smith (1988) at high winds. However, there is increasing evidence from shipboard observations (e.g., those that were used to develop COARE 3.0) that measured drag coefficients are significantly larger than these parameterizations over the open ocean. Direct covariance and mean wind measurements from ship-based observations suffer from flow distortion and imperfect motion correction (Edson et al. 1998), which is why the investigation described here has focused on data from fixed towers and low-profile platforms designed to minimize flow distortion.

Nonetheless, recent observational studies and numerical model predictions indicate that the drag coefficient should level off and even decrease at extreme wind conditions in order for hurricanes to develop. A Charnock coefficient that continues to increase with increasing winds does not support those observations and predictions. However, although the data are sparse above $22 \, \mathrm{m \, s^{-1}}$ in this study, the values of the Charnock coefficient shown in Fig. 6 indicate that they level off at $\alpha \approx 0.028$ around $19 \, \mathrm{m \, s^{-1}}$. This slows the increase of the drag coefficient above $19 \, \mathrm{m \, s^{-1}}$ in agreement with measurements.

These results are consistent with the recent investigations by Foreman and Emeis (2010) and Andreas et al. (2012), which provide insight into the asymptotic behavior of the drag coefficient at extreme winds. In their approach, the drag coefficient is determined by a fit of the friction velocity to the wind speed for wind speeds that correspond to fully rough seas. This approach is used to produce the result shown in Fig. 10, where the friction velocity is plotted against U_{10N}. This plot shows how the regime change from smooth to fully rough impacts the behavior of the friction velocity (and surface stress) with increasing winds. The data suggest that the transition from smooth to rough occurs over a wind speed range between 4 and $8.5 \, \mathrm{m \, s^{-1}}$ where the friction velocity is closely approximately by the first guess used in the COARE algorithm, that is, $u_* = 0.035 U_{10N}$.

The data above $8.5 \, \mathrm{m \, s^{-1}}$ are considered fully rough and a fit to this data is given by

$$u_* = C_m U_{10N} + u_{*0}, \qquad (22)$$

where $C_m = 0.062$ and $u_{*0} = -0.28$. This result is remarkably similar to the recently investigation by Andreas et al. (2012) that reported values of $C_m = 0.058$ and $u_{*0} = -0.24$. This function can be rearranged to provide the more traditional form of the drag coefficient

$$C_{D10N} = \left(\frac{u_*}{U_{10N}} \right)^2 = \left(C_m + \frac{u_{*0}}{U_{10N}} \right)^2, \qquad (23)$$

which is plotted in the lower panel of Fig. 10. This function predicts the increase of the drag coefficient to slow as a result of the intercept and ultimately asymptotes to a value of $10^3 \times C_m^2 \approx 3.8$. While this value is much larger than those inferred from aircraft observations in hurricanes (Black et al. 2007), the value of $10^3 \times C_{D10N} \approx 2.8$ at $30 \, \mathrm{m \, s^{-1}}$ falls well within the observations and suggested parameterizations reported by Powell et al. (2003). Therefore, although this formulation is not expected to hold for wind speeds associated with tropical cyclones, it provides additional evidence that the increase of the drag coefficient with winds is already slowing between 20 and $25 \, \mathrm{m \, s^{-1}}$.

b. Low wind speeds

The bin-averaged drag coefficients fall below both the COARE 3.0 and 3.5 parameterization at the lowest wind speed (e.g., $U_{10N} < 4 \, \mathrm{m \, s^{-1}}$; Fig. 6). This discrepancy is slightly larger in the CBLAST dataset (Edson et al. 2007), which was almost always swell dominated at low wind speeds. Swell moving faster than the wind provides momentum to the atmosphere, which acts to reduce the drag and the total momentum flux. This has been supported by the large-eddy simulations of wind–swell interaction reported by Sullivan et al. (2008). The LES results indicate that the dominant forces above the waves in this region are a wave-induced momentum flux divergence that accelerates the flow and a retarding pressure gradient, that is, opposite to the momentum balance in classical boundary layers. Under these conditions, the wave-driven winds produce a low-level jet and a rapid decay of the momentum flux with height.

This upward exchange of momentum as a result of wave-driven winds (Hanley and Belcher 2008) is expected to reduce the total momentum flux, which would act to reduce the drag under these conditions. As a result, the roughness appears smoother than the smooth-flow conditions measured under laboratory conditions.
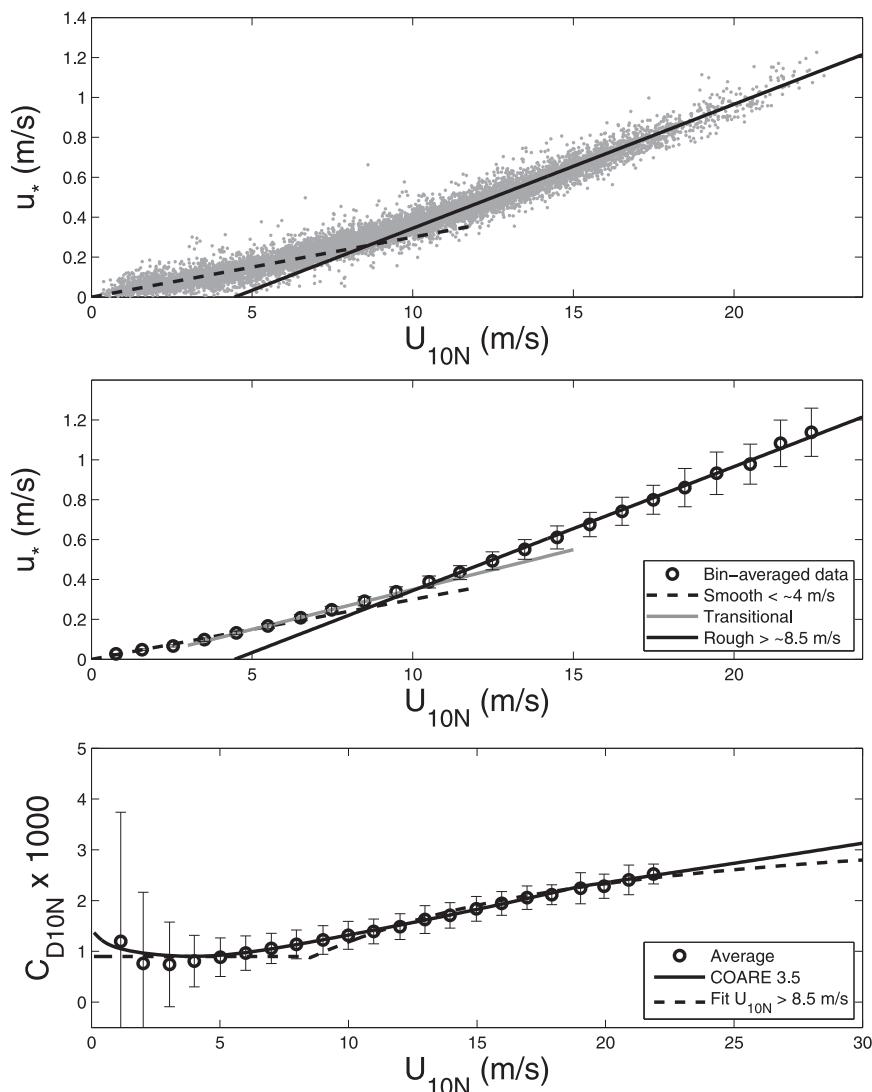
FIG. 10. (top) Individual estimates of friction velocity vs relative wind speed and (middle) their wind speed bin averages. The dashed line is equal to $u_* = 0.03U_{10N}$, the solid gray line is a fit to the data $4 \, \mathrm{m \, s^{-1}} < U_{10N} < 8.5 \, \mathrm{m \, s^{-1}}$ that closely follows $u_* = 0.035U_{10N}$, and the solid black line is a fit to the data for $U_{10N} \geq 8.5 \, \mathrm{m \, s^{-1}}$. (bottom) As in Fig. 9, but with the addition of the dashed line representing the drag coefficient given by (23) that combines the high-wind speed fit with the smooth-flow value.

The impact of the upward momentum flux has been investigated in a number of studies including those by Drennan et al. (1999), Smedman et al. (1994, 1999, 2003), Grachev and Fairall (2001), Grachev et al. (2003), and Hanley and Belcher (2008). Therefore, there is a growing consensus that wind–swell interaction is the leading cause for the reduction of the drag on low winds (Hanley et al. 2010).

c. Flux comparison

This investigation is concluded with a comparison of the DC estimates of the friction velocity versus bulk estimates using wind speed–, wave age–, and wave slope–dependent parameterization of the Charnock coefficient using (13), (15), and (18), respectively, as shown in Fig. 11. The DC and bulk estimates from RASEX are also plotted to provide independent comparisons (i.e., using data that are not used to develop the parameterizations) and to test COARE 3.5 in a fetch-limited shallow water environment. The RASEX dataset is that used in Vickers and Mahrt (1999). However, the data for all values of the fetch are used in this comparison.

The performance of each parameterization is determined from the RMS difference between the direct
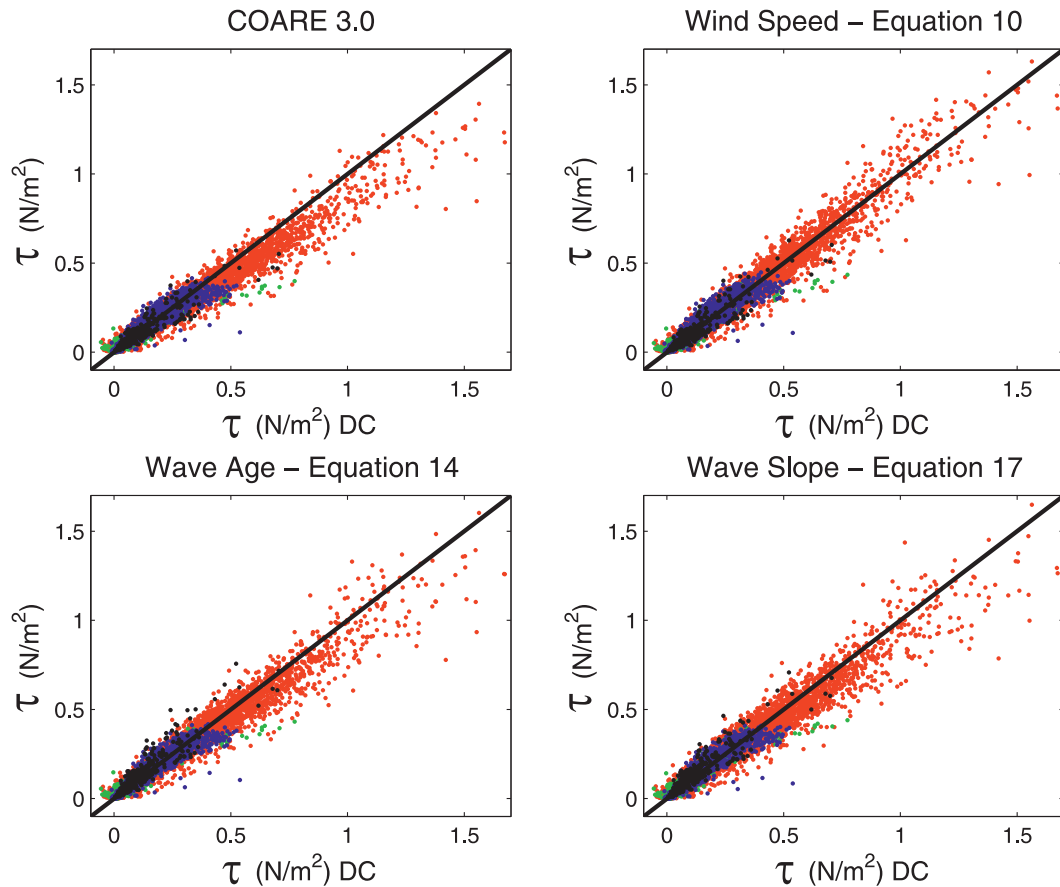
FIG. 11. Scatterplots of DC estimate of the surface stress vs (top) (left) the COARE 3.0 algorithm and (right) wind speed; and (bottom) (left) wave age, and (right) wave slope based parameterization developed in this study for COARE 3.5. The red points are from the CLIMODE buoy, the blue from MBL, the green from CBLAST, and the black from RASEX.

and bulk estimates of the flux. The overall RMS would be overwhelmed by the CLIMODE dataset because of its large size. Therefore, the RMS is computed from the individual datasets and then averaged. These results are summarized in Table 1, where we have added the Smith et al. (1992) and Donelan (1990) parameterizations for comparison.

The results show that the wind speed–dependent formulation is most accurate for the open-ocean datasets. This is true for both the average and individual datasets suggesting that the wind speed–dependent formulation in COARE 3.5 is an improvement over COARE 3.0 even at the lower wind speeds experienced in CBLAST and MBL. The wind speed–dependent formulation also gives the best agreement with the RASEX data. The wave slope–dependent formulation is slightly more accurate than the wave age–dependent formulation. However, all of the formulations developed in this investigation give similar agreement over the wide range of wind speed, wave age, and wave slopes found in the combined datasets.

4. Summary

The combination of data collected over a wide range of wind speed, sea state, and atmospheric stability conditions during the RASEX, MBL, CBLAST, and CLIMODE programs is used to improve parameterization of the drag coefficient over the ocean. All of these programs measured the momentum, heat, and mass fluxes directly using the DC method. The RASEX, MBL, and CBLAST programs also measured wind profiles to estimate the dimensionless shear over the ocean. The combined dataset is in good agreement with the dimensionless shear formulation used in COARE 3.0 that is based on over-land and over-ice experiments. The dimensionless shear shows little influence of the waves on the wind profiles above 4 m indicating that the measurements are above the WBL for momentum—at least for $c_p/U_{10N} < 2.5$.

The study then investigates the behavior of the surface roughness and drag coefficients at high wind speed

TABLE 1. The RMS difference between the directly measured stress and estimates using COARE 3.0 and the wind speed–, wave age–, and wave slope–dependent parameterizations developed in this study for inclusion in COARE 3.5. The average is the mean of the values from the three experiments used to develop the parameterizations and the RASEX program is included as an independent test. The percent uncertainty represents the average RMS divided by the average mean ($\times$ 100) Results based on the parameterizations reported by Smith et al. (1992) and Donelan (1990) are provided for comparison.

	Mean	COARE 3.0 RMS	Wind speed RMS	Wave age RMS	Wave slope RMS	Smith RMS	Donelan RMS
MBL/*FLIP* (N m^{-1})	0.131	0.0396	0.0393	0.0395	0.0394	0.0400	0.0410
RASEX (N m^{-1})	0.118	0.0414	0.0412	0.0483	0.0442	0.0483	0.0442
CBLAST-LOW (N m^{-1})	0.043	0.0200	0.0183	0.0190	0.0187	0.0184	0.0182
CLIMODE (N m^{-1})	0.198	0.0531	0.0425	0.0479	0.0507	0.0588	0.0562
Average (N m^{-1})	0.122	0.0385	0.0353	0.0386	0.0382	0.0414	0.0399
Uncertainty (%)		31.5	28.9	31.6	31.3	33.8	32.6%

using data collected during the CLIMODE program. The new data resulted in minor changes to the wind speed–dependent Charnock coefficient used in the COARE 3.0 algorithm at wind speeds over $13 \, \mathrm{m \, s^{-1}}$. These modifications are included in the COARE 3.5 algorithm, which gives good agreement with the stress estimates collected under a wide range of wind and wave conditions during the CBLAST, MBL, RASEX, and CLIMODE programs.

Numerous investigations have shown that the Charnock coefficient is also dependent on the state of the surface wave field. Therefore, the combined dataset is used to develop wave age– and wave slope–dependent parameterizations of the surface roughness, which are included in COARE 3.5. These parameterizations also give good agreement with the directly measured momentum fluxes over a wide range of sea states and wave ages. However, the COARE 3.5 wind speed–dependent formulation is shown to provide better agreement with the DC stress measurements without any wave information. Furthermore, it is nearly identical to the function representing the globally averaged drag coefficient from a wave age–based model run at the ECMWF.

These findings are easily reconciled using the observed linear relationship between wind speed and inverse wave age over the open ocean. The reason for this is found in the wind and wave data; namely, in storm passage after storm passage, the wave age varies nearly linearly with wind speed. The composite of all these storms shows that young waves are almost always found under high wind conditions, and old waves are found in their wake after winds have calmed down. Therefore, there is not a pronounced functional difference between drag coefficients based on wind speed and on wave age over the open ocean up to approximately $25 \, \mathrm{m \, s^{-1}}$.

It is fair to ask if the observations used in this analysis are representative of the entire ocean, since they were mainly taken in midlatitudes. However, the good agreement between the observations and the ECMWF globally averaged fields suggest that the COARE 3.5 parameterization can be used to give accurate momentum fluxes over the open ocean, with the greatest uncertainty at low wind speeds in the presence of swell. However, the ubiquitous nature of swell (e.g., Hanley et al. 2010) and its overall tendency to reduce the total momentum flux argues for a parameterization that reduces the drag compared to COARE 3.0 under light wind conditions.

It is also evident that the nearly linear relationship between wind speed and inverse wave age breaks down in the fetch-limited and shallow-water environment that characterized the RASEX program as shown in Fig. 9. However, the wave age– and wave slope–dependent parameterizations of the Charnock coefficient give good agreement with the directly measured fluxes for all of the field programs including RASEX. Although these functions are tuned to data with infinite fetch used in this analysis, this implies that the parameterizations are applicable to a wide range of marine environments.

Lastly, the results argue that it is difficult to improve upon a wind speed–dependent parameterization under any conditions. This may simply be due to the fact that wind-driven waves support the majority of the surface stress, and the modulation of the surface stress by longer waves is a second-order effect under most conditions. Furthermore, the inclusion of additional dependent variables with their own measurement uncertainties in the bulk flux algorithm tends to increase the uncertainties in the fluxes. Therefore, the potential improvements from the wave age– and wave slope–dependent parameterizations may be better utilized in applications where higher quality wave measurements are available.
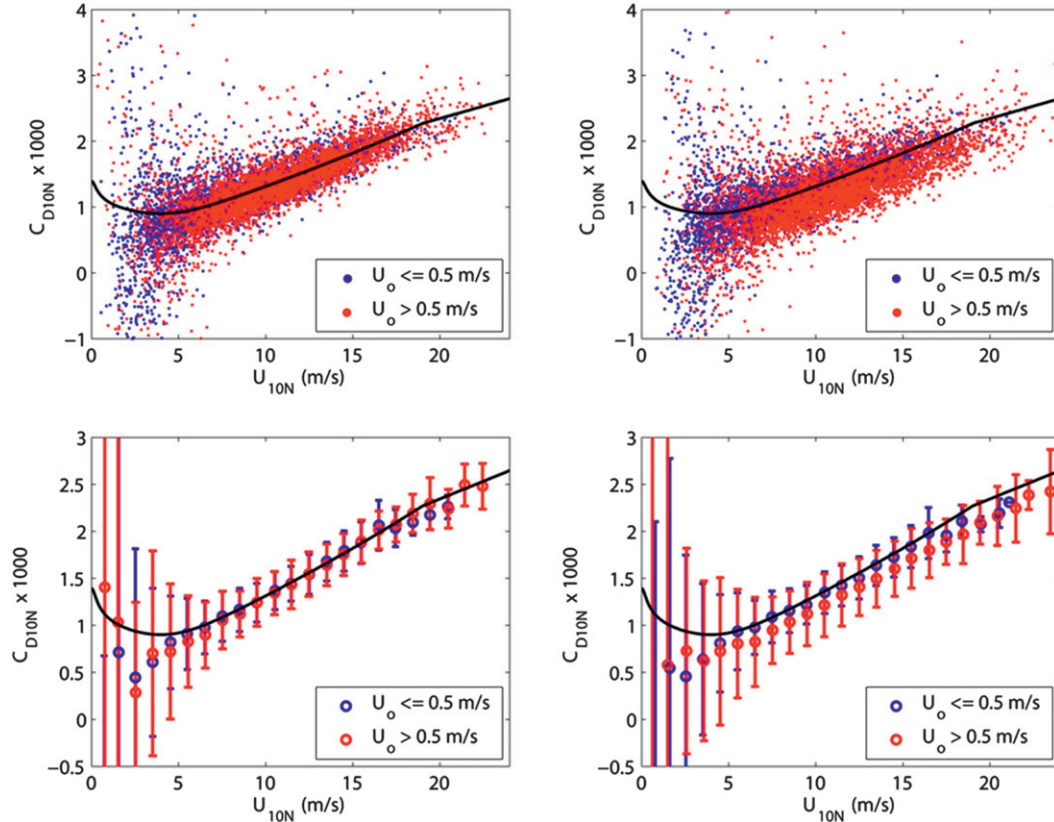
FIG. A1. Drag coefficient vs wind speed for the COARE 3.5 algorithm computed using (left) relative winds and (right) absolute winds. (top) Individual direct-covariance stress estimates and (bottom) bin-averaged values. Colors indicate relatively small (blue) and large (red) sea surface current speeds that correspond to the buoys being located outside and within the Gulf Stream, respectively.

APPENDIX

Relative Wind Speed

The wind speed relative to the ocean surface is required to properly estimate the surface fluxes of momentum, heat, and mass. For example, the wind stress τ at the sea surface can be parameterized as

$$\tau = -\rho_a \overline{uw} \cong \rho_a C_D U_r^2, \tag{A1}$$

where ρ_a is the density of air; $\rho_a \overline{uw}$ represents the flux computed using the DC method where u and w are the fluctuating along-wind and vertical velocity components, respectively, where the overbar denotes a time average; C_D is the drag coefficient; and U_r is the mean wind speed relative to water (i.e., the air–water velocity difference). For example, on a surface mooring, the relative wind speed can be computed from

$$U_r = [(U_e - U_{0e})^2 + (U_n - U_{0n})]^{1/2}, \tag{A2}$$

where the subscripts e and n denote the easterly and northerly wind components, respectively, and the subscript 0 identifies the surface current components. The surface currents are often neglected in over-ocean investigation of air–sea exchange based on the assumption that they are small compared to the surface winds. However, surface currents can be a significant fraction

of the wind speed in a direction correlated with the wind direction. For example, western boundary currents such as the Gulf Stream and Kuroshio often have components that are aligned with the predominant wind direction. More generally, wind-driven currents are inherently in the direction of the wind. Therefore, the wind speed relative to the ocean is systematically lower, on average, than the wind speed relative to fixed Earth by a few percent. This is true for all wind speeds, that is, not just under low wind conditions.

The CLIMODE dataset taken in the vicinity of the Gulf Stream is a good dataset to demonstrate the importance of including U_0 to calculate the drag coefficient and wind stress. For example, neutral drag coefficients computed using direct covariance fluxes with relative versus fixed-Earth wind speeds are shown in Fig. A1. When C_{DN} is computed using relative wind, the data collapse to a consistent fit that is independent of surface current speed. When C_{DN} is computed using absolute wind, there is a reduction in drag for strong currents, consistent with a significant fraction of the current being, on average, in the direction of the wind blowing over the Gulf Stream. Although more subtle, it is interesting to note that fixed-Earth C_{DN} are also systematically lower than the relative C_{DN} even when the buoy is outside the meandering Gulf Stream. This is due to the systematic reduction of the relative wind speeds resulting from wind-driven currents, which act to increase C_{DN} computed with the relative wind speed (i.e., by dividing the flux with a smaller value of the wind speed). More importantly, the collapse of the C_{DN} data and reduction of the scatter using relative winds indicates that the combination of this formulation with relative winds provides the most accurate estimate of the fluxes.

REFERENCES

Andreas, E. L, L. Mahrt, and D. Vickers, 2012: A new drag relation for aerodynamically rough flow over the ocean. *J. Atmos. Sci.,* **69,** 2520–2537.

Banner, M. L., and W. L. Peirson, 1998: Tangential stress beneath wind-driven air-water interfaces. *J. Fluid Mech.,* **364,** 115–145.

Belcher, S. E., and J. C. R. Hunt, 1993: Turbulent shear flow over slowly moving waves. *J. Fluid Mech.,* **251,** 109–148.

Beljaars, A. C. M., and A. A. M. Holtslag, 1991: Flux parameterization over land surfaces for atmospheric models. *J. Appl. Meteor.,* **30,** 327–341.

Bigorre, S., R. A. Weller, J. Lord, J. B. Edson, and J. D. Ware, 2013: A surface mooring for air–sea interaction research in the Gulf Stream. Part II: Analysis of the observations and their accuracies. *J. Atmos. Oceanic Technol.,* **30,** 450–469.

Black, P. G., and Coauthors, 2007: Air–sea exchange in hurricanes: Synthesis of observations from the coupled boundary layer air–sea transfer experiment. *Bull. Amer. Meteor. Soc.,* **88,** 357–374.

Bourassa, M. A., D. G. Vincent, and W. L. Wood, 1999: A flux parameterization including the effects of capillary waves and sea state. *J. Atmos. Sci.,* **56,** 1123–1139.

Businger, J. A., 1988: A note on the Businger–Dyer profiles. *Bound.-Layer Meteor.,* **42,** 145–151.

——, J. C. Wyngaard, Y. Izumi, and E. F. Bradley, 1971: Flux profile relationships in the atmospheric surface layer. *J. Atmos. Sci.,* **28,** 181–189.

Chalikov, D. V., 1986: Numerical simulation of the boundary layer above waves. *Bound.-Layer Meteor.,* **34,** 63–98.

——, 1995: The parameterization of the wave boundary layer. *J. Phys. Oceanogr.,* **25,** 1335–1349.

——, and S. Rainchik, 2011: Coupled numerical modeling of wind and waves and the theory of the wave boundary layer. *Bound.-Layer Meteor.,* **138,** 1–41.

Charnock, H., 1955: Wind stress on a water surface. *Quart. J. Roy. Meteor. Soc.,* **81,** 639–640.

Dobson, F. W., S. D. Smith, and R. J. Anderson, 1994: Measuring the relationship between wind stress and sea state in the open ocean in the presence of swell. *Atmos.–Ocean,* **32,** 237–256.

——, R. J. Anderson, P. K. Taylor, and M. J. Yelland, 1999: Storm Wind Study II: Open ocean wind and sea state measurements. *Proceedings of Symposium on the Wind-Driven Air–Sea Interface: Electromagnetic and Acoustic Sensing, Wave Dynamics and Turbulent Fluxes,* M. L. Banner, Ed., University of New South Wales, 295–296.

Donelan, M. A., 1990: Air–sea interaction. *The Sea,* B. LeMehaute and D. M. Hanes, Eds., *Ocean Engineering Science,* Vol. 9, Wiley and Sons, 239–292.

——, M. G. Skafel, H. Graber, P. Liu, D. Schwab, and S. Venkatesh, 1992: On the growth rate of wind-generated waves. *Atmos.–Ocean,* **30,** 457–478.

——, F. W. Dobson, S. D. Smith, and R. J. Anderson, 1993: On the dependence of sea surface roughness on wave development. *J. Phys. Oceanogr.,* **23,** 2143–2149.

Drennan, W. M., H. C. Graber, and M. A. Donelan, 1999: Evidence for the effects of swell and unsteady winds on marine wind stress. *J. Phys. Oceanogr.,* **29,** 1583–1864.

——, P. K. Taylor, and M. J. Yelland, 2005: Parameterizing the sea surface roughness. *J. Phys. Oceanogr.,* **35,** 835–848.

Edson, J. B., and C. W. Fairall, 1998: Similarity relationships in the marine atmospheric surface layer for terms in the TKE and scalar variance budgets. *J. Atmos. Sci.,* **55,** 2311–2328.

——, A. A. Hinton, K. E. Prada, J. E. Hare, and C. W. Fairall, 1998: Direct covariance flux estimates from mobile platforms at sea. *J. Atmos. Oceanic Technol.,* **15,** 547–562.

——, C. J. Zappa, J. A. Ware, W. R. McGillis, and J. E. Hare, 2004: Scalar flux profile relationships over the open ocean. *J. Geophys. Res.,* **109,** C08S09, doi:10.1029/2003JC001960.

——, and Coauthors, 2007: The Coupled Boundary Layers and Air–Sea Transfer Experiment in low winds. *Bull. Amer. Meteor. Soc.,* **88,** 341–356.

Fairall, C. W., E. F. Bradley, D. P. Rogers, J. B. Edson, and G. S. Young, 1996: Bulk parameterization of air–sea fluxes for TOGA COARE. *J. Geophys. Res.,* **101,** 3747–3764.

——, ——, J. E. Hare, A. A. Grachev, and J. B. Edson, 2003: Bulk parameterization of air–sea fluxes: Updates and verification for the COARE algorithm. *J. Climate,* **16,** 571–591.

Foreman, R. J., and S. Emeis, 2010: Revisiting the definition of the drag coefficient in the marine atmospheric boundary layer. *J. Phys. Oceanogr.,* **40,** 2325–2332.

Friehe, C. A., J. A. Smith, K. F. Rieder, N. E. Huang, J.-P. Giovanangeli, and G. L. Geernaert, 2001: Wind, stress and wave directions. *Wind Stress over the Ocean,* I. S. F. Jones and Y. Toba, Eds., Cambridge University Press, 232–241.

Geernaert, G. L., K. B. Katsaros, and K. Richter, 1986: Variation of the drag coefficient and its dependence on sea state. *J. Geophys. Res.,* **91** (C6), 7667–7679.

Grachev, A. A., and C. W. Fairall, 2001: Upward momentum transfer in the marine boundary layer. *J. Phys. Oceanogr.,* **31,** 1698–1711.

——, ——, J. E. Hare, J. B. Edson, and S. D. Miller, 2003: Wind stress vector over ocean waves. *J. Phys. Oceanogr.,* **33,** 2408–2429.

Hanley, K. E., and S. E. Belcher, 2008: Wave-driven wind jets in the marine atmospheric boundary layer. *J. Atmos. Sci.,* **65,** 2646–2660.

——, ——, and P. P. Sullivan, 2010: A global climatology of wind–wave interaction. *J. Phys. Oceanogr.,* **40,** 1263–1282.

Hare, J. E., T. Hara, J. B. Edson, and J. M. Wilczak, 1997: A similarity analysis of the structure of air flow over surface waves. *J. Phys. Oceanogr.,* **27,** 1018–1037.

Hersbach, H., 2011: Sea surface roughness and drag coefficient as functions of neutral wind speed. *J. Phys. Oceanogr.,* **41,** 247–251.

Hicks, B. B., 1978: Some limitations of dimensional analysis and power laws. *Bound.-Layer Meteor.,* **14,** 567–569.

Hristov, T. S., S. D. Miller, and C. A. Friehe, 2003: Dynamical coupling of wind and ocean waves through wave-induced air flow. *Nature,* **422,** 55–58.

Hsu, S. A., 1974: A dynamic roughness equation and its application to wind stress determination at the air–sea interface. *J. Phys. Oceanogr.,* **4,** 116–120.

Johnson, H. K., and H. Kofoed-Hansen, 2000: Influence of bottom friction on sea surface roughness and its impact on shallow water wind wave modeling. *J. Phys. Oceanogr.,* **30,** 1743–1756.

——, and H. J. Vested, 1992: Effects of water waves on wind shear stress for current modeling. *J. Atmos. Oceanic Technol.,* **9,** 850–861.

——, J. Højstrup, H. J. Vested, and S. E. Larsen, 1998: On the dependence of sea surface roughness on wind waves. *J. Phys. Oceanogr.,* **28,** 1702–1716.

Kitaigorodskii, S. A., 1973: *The Physics of Air–Sea Interaction.* Cambridge University Press, 273 pp.

Kraus, E. B., and J. A. Businger, 1994: *Atmosphere-Ocean Interaction.* Oxford University Press, 362 pp.

Kudryavtsev, V. N., V. K. Makin, and J. F. Meirink, 2001: Simplified model of the air flow above the waves. *Bound.-Layer Meteor.,* **100,** 63–90.

Lange, B., H. K. Johnson, S. Larsen, J. Højstrup, H. Kofoed-Hansen, and M. J. Yelland, 2004: On detection of a wave age dependency for the sea surface roughness. *J. Phys. Oceanogr.,* **34,** 1441–1458.

Large, W. G., and S. Pond, 1981: Open ocean momentum flux measurements in moderate to strong winds. *J. Phys. Oceanogr.,* **11,** 324–336.

Liu, W. T., K. B. Katsaros, and J. A. Businger, 1979: Bulk parameterization of air–sea exchanges of heat and water vapor including the molecular constraints at the interface. *J. Atmos. Sci.,* **36,** 1722–1735.

Mahrt, L., D. Vickers, J. Howell, J. Højstrup, J. M. Wilczak, J. B. Edson, and J. E. Hare, 1996: Sea surface drag coefficients in RASEX. *J. Geophys. Res.,* **101,** 14 327–14 335.

——, ——, J. Edson, J. Sun, J. Højstrup, J. Hare, and J. Wilczak, 1998: Heat flux in the coastal zone. *Bound.-Layer Meteor.,* **86,** 421–446.

——, ——, ——, J. Wilczak, J. Hare, and J. Højstrup, 2001: Vertical structure of offshore flow during RASEX. *Bound.-Layer Meteor.,* **100,** 47–61.

Marshall J., and Coauthors, 2009: Observing the cycle of convection and restratification over the Gulf Stream system and the subtropical gyre of the North Atlantic Ocean: Preliminary results from the CLIMODE field campaign. *Bull. Amer. Meteor., Soc.,* **90,** 1337–1350.

Martin, M. J., 1998: An investigation of momentum exchange parameterizations and atmospheric forcing for the coastal mixing and optics program. M.S. thesis, Massachusetts Institute of Technology, Boston, MA, and the Woods Hole Oceanographic Institution, Woods Hole, MA, 83 pp.

Mastenbroek, C. V., V. K. Makin, M. H. Garrat, and J. P. Giovanangeli, 1996: Experimental evidence of the rapid distortion of the turbulence in the air flow over water waves. *J. Fluid Mech.,* **318,** 273–302.

Miles, J. W., 1957: On the generation of surface waves by shear flows. *J. Fluid Mech.,* **3,** 185–204.

Miller, S. D., T. S. Hristov, J. B. Edson, and C. A. Friehe, 2008: Platform motion effects on measurements of turbulence and air–sea exchange over the open ocean. *J. Atmos. Oceanic Technol.,* **25,** 1683–1694.

Monin, A. S., and A. M. Obukhov, 1954: Basic laws of turbulent mixing in the surface layer of the atmosphere. *Tr. Geofiz. Inst., Akad. Nauk SSSR,* **151,** 163–187.

Moon, I.-J., T. Hara, I. Ginis, S. E. Belcher, and H. L. Tolman, 2004: Effect of surface waves on air–sea momentum exchange. Part I: Effect of mature and growing seas. *J. Atmos. Sci.,* **61,** 2321–2333.

Nordeng, T. E., 1991: On the wave age dependent drag coefficient and roughness length at sea. *J. Geophys. Res.,* **96,** 7167–7174.

Obukhov, A. M., 1971: Turbulence in an atmosphere with a non-uniform temperature. *Bound.-Layer Meteor.,* **2,** 7–29.

Oost, W. A., G. J. Komen, C. M. J. Jacobs, and C. van Oort, 2002: New evidence for a relation between wind stress and wave age from measurements during ASGAMAGE. *Bound.-Layer Meteor.,* **103,** 409–438.

Persson, O. G. P., C. W. Fairall, E. L Andreas, P. S. Guest, and D. K. Perovich, 2002: Measurements near the atmospheric surface flux group tower at SHEBA: Near-surface conditions and surface energy budget. *J. Geophys. Res.,* **107,** 8045, doi:10.1029/2000JC000705.

Plant, W. J., 1982: A relationship between wind stress and wave slope. *J. Geophys. Res.,* **87,** 1961–1967.

Powell, M. D., P. J. Vickery, and T. A. Reinhold, 2003: Reduced drag coefficient for high wind speeds in tropical cyclones. *Nature,* **422,** 279–283.

Smedman, A. S., M. Tjernström, and U. Högström, 1994: The near-neutral marine atmospheric boundary layer with no surface shearing stress: a case study. *J. Atmos. Sci.,* **51,** 3399–3411.

——, U. Högström, H. Bergström, A. Rutgersson, K. K. Kahma, and H. Pettersson, 1999: A case study of air–sea interaction during swell conditions. *J. Geophys. Res.,* **104** (C11), 25 833–25 852.

——, X. G. Larsén, U. Högström, K. K. Kahma, and H. Pettersson, 2003: Effect of sea state on the momentum exchange over the sea during neutral conditions. *J. Geophys. Res.,* **108,** 3367, doi:10.1029/2002JC001526.

Smith, S. D., 1988: Coefficients for sea surface wind stress, heat flux, and wind profiles as a function of wind speed and temperature. *J. Geophys. Res.,* **93** (C12), 15 467–15 472.

——, and Coauthors, 1992: Sea surface wind stress and drag coefficients: The HEXOS results. *Bound.-Layer Meteor.,* **60,** 109–142.

Sullivan, P. P., J. B. Edson, T. Hristov, and J. C. McWilliams, 2008: Large-eddy simulations and observations of atmospheric marine boundary layers above non-equilibrium surface waves. *J. Atmos. Sci.,* **65,** 1225–1245.

Taylor, P. K., and M. J. Yelland, 2001: The dependence of sea surface roughness on the height and steepness of the waves. *J. Phys. Oceanogr.,* **31,** 572–590.

Vickers, D., and L. Mahrt, 1999: Observations of non-dimensional wind shear in the coastal zone. *Quart. J. Roy. Meteor. Soc.,* **125,** 2685–2702.

Webster, P. J., and R. Lukas, 1992: TOGA COARE: The coupled ocean–atmosphere response experiment. *Bull. Amer. Meteor. Soc.,* **73,** 1377–1416.

Weller, R. A., S. P. Bigorre, J. Lord, J. D. Ware, and J. B. Edson, 2012: A surface mooring for air–sea interaction research in the Gulf Stream. Part I: Mooring design and instrumentation. *J. Atmos. Oceanic Technol.,* **29,** 1363–1376.